A Nonlinear Filter for Real-Time Joint Tracking and Recognition

Keith Kastella[1]
Lockheed-Martin Tactical Defense Systems, Eagan

Aleksandar Zatezalo[2]
University of Minnesota

Abstract: This paper presents an approach to non-cooperative aircraft identification that uses non-linear filtering to fuse target kinematic state measurements and target signature measurements. This is applicable to sensors whose signature measurements are sensitive to the sensor-target orientation such as high range resolution radar, synthetic aperture radar, ladar and electo-optical imagers. Fusion is achieved by constructing the joint density for the target's kinematic state and its class, conditioned on the data. The marginal density for the target class is obtained by integrating out the kinematic variables in this joint density, enabling target recognition. This process is inherently non-Gaussian due to non-linear target dynamics and the presence of multiple modes in the signature densities. To model these non-linearities the time evolution of the joint density between measurements is determined by solving the Fokker-Planck equation using the Alternating Direction Implicit method, a fast finite difference partial differential equation solver. As measurements become available, they are used to update the joint kinematic/class density using Bayes rule and densities derived from physical sensor models. This preserves the non-Gaussian features of the joint density including feedback between aspect, kinematics and class. In a test problem fusing simulated position measurements with high range resolution radar signatures this reduces time-to-classify compared with a Maximum Likelihood Classifier that does not use the position measurements.

Keywords: Non-linear filtering, automatic target recognition, joint tracking and recognition, high range resolution radar

1. Introduction

The goal of Non-Cooperative Target Identification (NCTI) is to estimate target class of an object (e.g. F-16 or A-10) given a set of measurements. Many types of sensors have been proposed for NCTI applications including imaging sensors and High Range Resolution Radar (HRR), both of which are sensitive to the aspect angle of the target relative to the sensor. For many types of targets, especially airborne ones, target motion is strongly

[1] Supported by the Minnesota Center for Industrial Research under Airforce Office of Scientific Research grant F49620-96-1-0382 and by the Lockheed-Martin internal research and development program.
[2] Supported by the Minnesota Center for Industrial Research and by the Lockheed-Martin internal research and development program.

Submitted to IEEE Transactions on Aerospace and Electronic Systems, December 31, 1997

correlated with target orientation (also referred to as target pose or aspect). For this reason signature measurements also contain information concerning the target's kinematic states such as position, velocity, bank and pitch angles. For example, if an aircraft is turning, it is usually banked. A turn is said to be coordinated if the target bank angle is such that the sum of the centrifugal force and gravity always presses the pilot straight down into her seat. In this case the bank angle is determined by the speed and turn rate. The goal of this paper is to exploit this correlation to improve the performance of NCTI systems.

Although the method proposed here is applicable to any sensor whose signatures are aspect-dependent, this paper will focus on applications to HRR. Recent overviews of HRR based NCTI include [Smith, Mitchell1, Zyweck]. HRR uses broad-bandwidth linear frequency modulation or step frequency waveforms to measure range profiles ("signatures") of targets. Prototype systems tested against airborne targets have sub-meter resolution [Wehner, Berman]. In HRR systems the range profile is a list of scattering intensities as a function of range. This intensity is related to the cross-range-integrated scattering cross-section of the target at that range cell. Since the scattering into a particular range cell comes from many points of the target, it is sensitive to the orientation angle from which the target is observed. [Iny] have examined the variation of HRR data with target pose, stores and articulation and suggest that good performance can be achieved using a few signatures per square degree of solid angle, although this also depends on the center frequency of the RADAR system. With one signature per solid-angle degree, on the order of 10^4 signatures per class are required, suggesting that large computational and storage resources are required for good NCTI. The range- and pose-dependence of the range profile statistics are nonlinear. For example, there may be multiple target classes and/or target aspects that fit a particular range profile. For such range profiles, the posterior probability for target pose conditioned on the profile is multi-modal.

The classical approach to target ID with HRR is to use a quadratic classifier [Fukunaga] based on synthetic or measured signature templates for a target-set over a large collection of poses [Mitchell-1, Iny, Smith]. Due to noise and the multimodel nature of the data, observations from several different poses must be used to classify targets reliably. As discussed in [Libby], this approach only uses the HRR data to estimate the target pose. One problem with this approach is that the maximum likelihood may be obtained by a physically unrealizable sequence of pose angles (e.g. a sequence of poses flipping between 0 and 180 degrees is not penalized), leading to misclassification of the target. On the other hand, if target class is known, then the HRR signatures contain useful information about target pose such as heading and bank angle, which can be used to infer kinematic quantities such as velocity and turn rate.

In practice HRR is often one of several modes available on a multimode radar system. To identify an object, the sensor can dwell on the target for a brief time, interleaving HRR pulse trains with other types of wave-forms optimized to measure the target's azimuth, elevation and radial velocity, which we refer to as kinematic measurements. In this case

the data stream consists of a mixture of nearly simultaneous signature and kinematic measurements. The theoretically optimal approach is to process the signature and kinematic data in a fully integrated estimator based on the joint density for the target class and kinematic state. This joint density can capture correlation information between class and kinematics, enhancing their mutual estimation. This is difficult to implement due to the difficulty of constructing this joint density. As a result, most systems perform kinematic state estimation first and then use the kinematic state estimate to aid target identification.

Several authors have suggested methods to improve tracking by exploiting the correlation between aircraft orientation and target acceleration [Kendrick, Andrisani, O'Sullivan, Miller]. Other researchers have developed systems that improve classification performance by using some type of kinematic information. Although they do not use kinematic measurements, [Le Chevalier, Mieras] utilize kinematic constraints in their classifiers by penalizing or excluding unrealistically large pose changes between signature measurements. Both [Libby] and [O'Sullivan] have proposed classification schemes to combine kinematic measurements with HRR and [Rozovski] use a similar strategy with electo-optical measurements.

For example, [Libby] extend the estimation approach of [Larson] to exploit aspect information for NCTI in an uncoupled feed-forward fashion as shown in Figure 1 a . Given Bayesian assumptions, the theoretically optimal approach to classification is to compute the posterior probability $p(T|Y)$ for target class T given a set of measurements Y. Then the minimum-probability-of-error classifier is obtained by selecting the class T to maximize $p(T|Y)$. [Libby] approximately solve this maximization problem by first using an extended Kalman filter and fixed-lag smoother to estimate the target trajectory from the kinematic measurements alone. Then they construct a jointly Gaussian pose sequence likelihood from this estimated trajectory, assuming that the target's turns are coordinated. Assuming statistical independence, [Libby] combine this pose sequence likelihood with the HRR measurement likelihood. Dynamic programming is then used to obtain the pose sequence that approximately maximizes the combined kinematic and HRR measurement likelihood. The class with the highest total signature/kinematic likelihood is selected as the class estimate, approximating the joint maximum likelihood classifier. In [Libby] the information flow goes from the kinematic estimation to the range profile classifier, as shown in Figure 1a, but there is no information flow from the HRR measurements back to the kinematic estimator.

In contrast to [Libby], [O'Sullivan] propose a batch algorithm that incorporates two-way coupling of kinematic and signature data elements. This closes the loop between classification, pose estimation, and tracking yielding a single unified system, illustrated in Figure 2b. [O'Sullivan] use a batch calculation scheme based on stochastic methods (somewhat similar to simulated annealing) known as a jump-diffusion process [Miller]. This approach is very appealing. One of the main motivations of this current work is to explore the feasibility of capturing this coupling in a recursive filtering scheme.

It is important to note that for NCTI, the kinematic states of the target are of no interest: they are purely nuisance variables. However, an intermediate step in both [Libby] and [O'Sullivan] uses maximum likelihood methods (dynamic programming and stochastic simulation) to estimate the kinematic states of the target. There is a very different alternative approach that avoids this intermediate step. This is to work directly with the target's conditional probability density [Ho, Sorensen, Jazwinski, Daum, Rozovski]. Since the target dynamics are Markov, the time-evolution of the target density is first order so it can be computed recursively. This is in marked contrast to the maximum likelihood or the conditional expectation for the state, which can only be computed recursively under restrictive assumptions on both target dynamics and measurement statistics. Shifting attention to the conditional density obviates the need for any type of multiple scan processing while modeling the intrinsically non-linear relationship between target signatures, kinematic states and target classes. If efficient methods can be found to compute the target's conditional density, then real-time recursive algorithms can be constructed that couple the kinematic and signature information into a single filter as shown in Figure 2b. Several methods have been proposed to evaluate the relevant densities including spectral methods [Rozovsky], approximations based on separation of variables [Daum], and convolution methods [Kouritzin, Kastella].

For problems with continuum target dynamics and discrete measurements, propagation of the conditional density can be accomplished by solving a Fokker-Plank Equation (FPE). Recently, [Zatezalo] examined several finite difference methods for solving a model FPE typical of tracking applications. The four solvers studied were: the Alternating Direction Implicit (ADI) scheme [Strikwerda]; the method of fractional steps [Yanenko]; an Euler explicit scheme [Strikwerda]; and a multigrid scheme [McCormick]. For this problem ADI and the method of fractional steps were found to be about two orders of magnitude more efficient than the Euler explicit and multigrid schemes. Motivated by this result, this paper explores the applicability of ADI for joint tracking and recognition applications.

The remainder of this paper is organized as follows. Section 2 presents algorithmic details Nonlinear Filtering for Joint Tracking and Recognition (NLFJTR) used to fuse kinematic measurements and signature measurements for NCTI. As in most filters there are two parts to the algorithm: a) prediction of the effect of deterministic and random target motion on the target probability distribution and b) modification of the distribution with measurements as they become available. The target motion is characterized by the Ito stochastic differential equation [Jazwinski]. The Ito equation determines the dynamic evolution for the target class / state density with a slight modification to account for the target class, given by a partial differential equation called the Fokker-Planck equation (FPE). In this work the target dynamics are modeled as motion in a 2D plane with a randomly varying turn rate, leading to a 5-dimensional target state representation. The resulting Fokker-Planck equation is discretized and solved on a 5-dimensional grid using the D'Yakonov finite difference scheme, which is a specific instance of a large class of methods called Alternating Direction Implicit (ADI) schemes [Strikwerda]. One useful feature of ADI is that the computation required to evaluate one time update of the scheme

is proportional to the number of nodes in the grid used to represent the solution. The FPE for filtering problems of this type usually has variables with first order derivatives but no second order derivatives. When this occurs, the FPE is said to be "degenerate" and requires special boundary conditions [Friedman]. In order to minimize the size of the required grid, it is spatially translated to maintain the target location near the grid center. A physical model for the measurement density is required in order to update the target density with measurements. We present a simple scattering center model for HRR signatures [Smith] with additive noise and model position measurements with Gaussian error. For evaluation and comparison we also developed a Maximum Likelihood Classifier (MLC) which in this case reduces to a Guassian classifier.

Following the method section, we present simulation results using NLFJTR and the MLC in Section 3. When the signature noise is very low, both classifiers provide similar classification performance. As the signature noise increases, the performance of the MLC degrades much more quickly than NLFJTR classifier. At intermediate values of signature noise NLFJTR provides reliable classification more quickly than the MLC. At high values of signature noise the MLC is unable to classify the target after 20 scans while NLFJTR classifies with high reliability, illustrating the utility of the kinematic measurements for NCTI. Section 4 discusses these results and suggests directions for future research.

2. Continuous-Discrete Filtering for Joint Tracking and Recognition

Our objective is to classify an airborne target from a sequence of measurements $\mathbf{y}_k$ made at discrete times t_k. In general these measurements can be HRR profiles, range-Doppler measurements, imaging measurements or some combination thereof. The target is a member of some target class T_c, $c = 1, \ldots, C$. Some of the measurements $\mathbf{y}_k$ are sufficiently class-dependent in some way to enable classification. The target dynamics are described by the Ito stochastic differential equation [Jazwinski] for the time-dependent target state $\mathbf{x}_t$

$$d\mathbf{x}_t = \mathbf{f}(\mathbf{x}_t, t)dt + \mathbf{G}(\mathbf{x}_t, t)d\beta_t, \quad t \geq t_0 \tag{1}$$

where $\mathbf{x}_t$ and $\mathbf{f}$ are n-vectors, $\mathbf{G}$ is an $n \times r$ matrix function and $\{\beta_t, t \geq t_0\}$ is an r-vector Brownian motion process with $E\{d\beta_t d\beta_t^{\mathrm{T}}\} = \mathbf{Q}(t)dt$. In general $\mathbf{f}$ and $\mathbf{G}$ depend upon the target class but this dependence is not made explicit here.

The observations up to time τ are denoted

$$Y_\tau = \{\mathbf{y}_l : t_l \leq \tau\}. \tag{2}$$

Using this notation, the Bayes-optimal classifier can be constructed from the joint conditional probability density $p(\mathbf{x}_t, T_c | Y_t)$. Given the normalized joint density, the class probability is

$$p(T_c|Y_t) = \int d\mathbf{x}_t \, p(\mathbf{x}_t, T_c|Y_t) \, . \tag{3}$$

Then the minimum error classifier is [Fukunaga]

$$\hat{T}_c = \arg\max_{T_c} \; p(T_c|Y_t) \, . \tag{4}$$

The minimum mean square error target state estimate $\hat{\mathbf{x}}_t$ is [Jazwinski]

$$\hat{\mathbf{x}}_t = \sum_c \int \mathbf{x}_t \; p(\mathbf{x}_t, T_c|Y_t) d\mathbf{x}_t \; . \tag{5}$$

Between observations the evolution of the conditional density is determined by the target dynamics as characterized by the Ito equation. As shown in [Jaz], the time evolution of the joint density between measurements is the solution to the Fokker-Planck equation (FPE)

$$\frac{\partial p}{\partial t}(\mathbf{x}_t, T_c|Y_{t_k}) = L(p), \quad t_k \le t < t_{k+1}, \tag{6}$$

where

$$L(p) \equiv -\sum_{i=1}^{n} \frac{\partial(\mathbf{f}_i p)}{\partial \mathbf{x}_i} + \frac{1}{2}\sum_{i,j=1}^{n} \frac{\partial^2 \left(p\left(\mathbf{G}\mathbf{Q}\mathbf{G}^{\mathrm{T}}\right)_{ij} \right)}{\partial \mathbf{x}_i \partial \mathbf{x}_j} \tag{7}$$

with initial condition given by $p(\mathbf{x}, t_k|Y_{t_k})$.

We assumed that the conditional density $p(\mathbf{y}_k|\mathbf{x}_{t_k}, T_c)$ for measurement $\mathbf{y}_k$ given target class T_c and target state $\mathbf{x}_{t_k}$ was known. Further, we assumed that any measurement noise was white. Then given a new observation $\mathbf{y}_k$, the updated conditional density $p(\mathbf{x}, t_k|Y_{t_k})$ is obtained from the predicted density $p(\mathbf{x}, t_k|Y_{t_{k-1}})$ using Bayes' rule:

$$p(\mathbf{x}_{t_k}, T_c|Y_{t_k}) = \frac{p(\mathbf{y}_k|\mathbf{x}_{t_k}, T_c) \, p(\mathbf{x}_{t_k}, T_c|Y_{t_{k-1}})}{\sum_{c'} \int p(\mathbf{y}_k|\mathbf{x}'_{t_k}, T_{c'}) \, p(\mathbf{x}'_{t_k}, T_{c'}|Y_{t_{k-1}}) d\mathbf{x}'_{t_k}} \, . \tag{8}$$

2.1 The Target Motion Model

In this study we assumed that the target motion was restricted to motion in a horizontal plane. For fixed-wing aircraft executing constant altitude coordinated turns the bank angle θ is determined by the turn rate ω and speed s by

$$\theta = \text{atan}(\omega s / g) \tag{9}$$

where g is the acceleration due to gravity. A simple model was selected to incorporate variable turn-rate and planar motion using the 5-dimensional state

$$\mathbf{x} = (x, \dot{x}, y, \dot{y}, \omega)^{\mathrm{T}} \tag{10}$$

with

$$\mathbf{f}(\mathbf{x}) = (\dot{x}, -\omega\dot{y}, \dot{y}, \omega\dot{x}, 0)^{\mathrm{T}}. \tag{11}$$

The velocity/turn-rate coupling in the 2nd and 4th components of **f** is explicitly non-linear. The target model was driven by a 3-dimensional Brownian noise process $\beta_t = (\beta_t^{\dot{x}}, \beta_t^{\dot{y}}, \beta_t^{\omega})^{\mathrm{T}}$ with

$$\mathbf{G} = \begin{pmatrix} 0 & 0 & 0 \\ 1 & 0 & 0 \\ 0 & 0 & 0 \\ 0 & 1 & 0 \\ 0 & 0 & 1 \end{pmatrix} \tag{12}$$

and

$$\mathbf{Q} = \begin{pmatrix} \sigma_{\dot{x}}^2 & 0 & 0 \\ 0 & \sigma_{\dot{y}}^2 & 0 \\ 0 & 0 & \sigma_{\omega}^2 \end{pmatrix} \tag{13}$$

The resulting FPE (Eq. (6)) was found to be

$$\frac{\partial p}{\partial t} = -\dot{x}\frac{\partial p}{\partial x} - \dot{y}\frac{\partial p}{\partial y} + \omega\dot{y}\frac{\partial p}{\partial \dot{x}} - \omega\dot{x}\frac{\partial p}{\partial \dot{y}} + \frac{\sigma_{\dot{x}}^2}{2}\frac{\partial^2 p}{\partial \dot{x}^2} + \frac{\sigma_{\dot{y}}^2}{2}\frac{\partial^2 p}{\partial \dot{y}^2} + \frac{\sigma_{\omega}^2}{2}\frac{\partial^2 p}{\partial \omega^2} \tag{14}$$

2.2 The D'Yakonov Finite Difference Scheme

We used the D'Yakonov finite difference scheme to solve Eq. (14) numerically. Space and time were discretized on a uniform grid with time resolution Δt and spatial resolution

$\Delta\mathbf{x} = (\Delta x, \Delta\dot{x}, \Delta y, \Delta\dot{y}, \Delta\omega)^{\mathrm{T}}$. In this subsection p denotes a continuum solution to the FPE while q denotes a function defined on the grid that approximates p. Defining the sub-operators

$$A_1 = -\dot{x}\frac{\partial}{\partial x}, \tag{15a}$$

$$A_2 = \frac{\sigma_{\dot{x}}^2}{2}\frac{\partial^2}{\partial \dot{x}^2} + \omega\dot{y}\frac{\partial}{\partial \dot{x}}, \tag{15b}$$

$$A_3 = -\dot{y}\frac{\partial}{\partial y}, \tag{15c}$$

$$A_4 = \frac{\sigma_{\dot{y}}^2}{2}\frac{\partial^2}{\partial \dot{y}^2} - \omega\dot{x}\frac{\partial}{\partial \dot{y}}, \tag{15d}$$

$$A_5 = \frac{\sigma_{\omega}^2}{2}\frac{\partial^2}{\partial \omega^2}, \tag{15e}$$

the FPE can be written as

$$\frac{\partial p}{\partial t} = \sum_i A_i p \tag{16}$$

where $p(\mathbf{x}, t)$ is a continuum solution to the FPE subject to an appropriate boundary condition. Discretizing in time but not in space, we abbreviate $p^k = p(\mathbf{x}, t_k)$. The Crank-Nicholson scheme [Strickwerda, Press] for the FPE is obtained by using a Taylor series in time for $p(\mathbf{x}, t_k + \Delta t/2)$, leading to

$$\frac{p^{k+1} - p^k}{\Delta t} = \frac{1}{2}\sum_i A_i p^{k+1} + \frac{1}{2}\sum_i A_i p^k + O\left((\Delta t)^2\right). \tag{17}$$

Rearranging terms leads to

$$\left(1 - \frac{\Delta t}{2}\sum_i A_i\right)p^{k+1} = \left(1 + \frac{\Delta t}{2}\sum_i A_i\right)p^k + O\left((\Delta t)^3\right). \tag{18}$$

In principal, this expression can be solved for p^{k+1} by inverting the operator $1 - (\Delta t/2)\sum_i A_i$, but direct inversion is computationally expensive. An expression that is equivalent to $O\left((\Delta t)^3\right)$ but much simpler to invert is obtained by using the operator identity

$$\prod_i \left(1 \pm \frac{\Delta t}{2} A_i\right) = 1 \pm \frac{\Delta t}{2} \sum_i A_i + \left(\frac{\Delta t}{2}\right)^2 \sum_{i<j} A_i A_j + O\left((\Delta t)^3\right). \quad (19)$$

(The operator order must be preserved on both sides of the equality for non-commuting operators such as A_3 and A_4). Rearranging Eq. (19) leads to

$$1 \pm \frac{\Delta t}{2} \sum_i A_i = \prod_i \left(1 \pm \frac{\Delta t}{2} A_i\right) - \left(\frac{\Delta t}{2}\right)^2 \sum_{i<j} A_i A_j + O\left((\Delta t)^3\right). \quad (20)$$

so Eq. (18) yields

$$\prod_i \left(1 - \frac{\Delta t}{2} A_i\right) p^{k+1} = \prod_i \left(1 + \frac{\Delta t}{2} A_i\right) p^k + \left(\frac{\Delta t}{2}\right)^2 \sum_{i<j} A_i A_j \left(p^{k+1} - p^k\right) + O\left((\Delta t)^3\right). \quad (21)$$

Further, because $p^{k+1} - p^k = O(\Delta t)$,

$$\prod_i \left(1 - \frac{\Delta t}{2} A_i\right) p^{k+1} = \prod_i \left(1 + \frac{\Delta t}{2} A_i\right) p^k + O\left((\Delta t)^3\right). \quad (22)$$

If $A_{i\Delta \mathbf{x}}$ is an $O\left((\Delta \mathbf{x})^2\right)$ discretization of A_i, then

$$\prod_i \left(1 - \frac{\Delta t}{2} A_{i\Delta \mathbf{x}}\right) p^{k+1} = \prod_i \left(1 + \frac{\Delta t}{2} A_{i\Delta \mathbf{x}}\right) p^k + O\left(\Delta t (\Delta \mathbf{x})^2\right) + O\left((\Delta t)^3\right), \quad (23)$$

and the grid function q defined by

$$\prod_i \left(1 - \frac{\Delta t}{2} A_{i\Delta \mathbf{x}}\right) q^{k+1} = \prod_i \left(1 + \frac{\Delta t}{2} A_{i\Delta \mathbf{x}}\right) q^k \quad (24)$$

approximates p to $O\left(\Delta t (\Delta \mathbf{x})^2\right) + O\left((\Delta t)^3\right)$.

To propagate the density, we must solve Eq. (24) for q^{k+1}. Let N_A denote the number of sub-operators in the FPE. Then the D'Yakonov [Strikwerda] scheme for Eq. (24) is

$$\tilde{q}^k = \prod_i \left(1 + \frac{\Delta t}{2} A_{i\Delta \mathbf{x}}\right) q^k \quad (25a)$$

$$\tilde{q}^{k+i/N_A} = \left(1 - \frac{\Delta t}{2} A_{i\Delta \mathbf{x}}\right)^{-1} \tilde{q}^{k+(i-1)/N_A}, \quad i = 1, \ldots, N_A \quad (25b)$$

$$q^{k+1} = \tilde{q}^{k+1} \tag{25c}$$

where $\tilde{q}^{k+i/N_A}$ are intermediate results. The essential point to note is that each factor $\left(1-\Delta t A_{i\Delta \mathbf{x}}/2\right)$ can be inverted separately, simplifying the calculation.

To discretize the A_i, we abbreviate $q(k\Delta t, x\pm\Delta x, \dot{x}, y, \dot{y}, \omega) = q_{x\pm1}$ with similar definitions for $q_{\dot{x}\pm1},\ldots,q_{\omega\pm1}$. We chose central differencing for the spatial derivatives, obtaining

$$A_{1\Delta \mathbf{x}} q = -\frac{\dot{x}}{2\Delta x}\left(q_{x+1} - q_{x-1}\right), \tag{26a}$$

$$A_{2\Delta \mathbf{x}} q = \frac{\sigma_{\dot{x}}^2}{2\Delta \dot{x}^2}\left(q_{\dot{x}+1} - 2q + q_{\dot{x}-1}\right) + \frac{\omega \dot{y}}{2\Delta \dot{x}}\left(q_{\dot{x}+1} - q_{\dot{x}-1}\right), \tag{26b}$$

$$A_{3\Delta \mathbf{x}} q = -\frac{\dot{y}}{2\Delta y}\left(q_{y+1} - q_{y-1}\right), \tag{26c}$$

$$A_{4\Delta \mathbf{x}} q = \frac{\sigma_{\dot{y}}^2}{2\Delta \dot{y}^2}\left(q_{\dot{y}+1} - 2q + q_{\dot{y}-1}\right) - \frac{\omega \dot{x}}{2\Delta \dot{y}}\left(q_{\dot{y}+1} - q_{\dot{y}-1}\right), \tag{26d}$$

$$A_{5\Delta \mathbf{x}} q = \frac{\sigma_{\omega}^2}{2\Delta \omega^2}\left(q_{\omega+1} - 2q + q_{\omega-1}\right). \tag{26e}$$

With this discretization, each operator $\left(1-(\Delta t/2)A_{i\Delta \mathbf{x}}\right)$ to be inverted is tridiagonal. We inverted these operators using Thomas's algorithm [Strikwerda] which has $O(N)$ complexity so that the total complexity of Eq. (25a-c) was $O(N)$.

2.3 Boundary Conditions

In order to solve the discretized FPE numerically it must be restricted to a finite domain leading to an initial-boundary value problem. The finite grid domain consists of the points $((i+i_0)\Delta x, (j+j_0)\Delta \dot{x}, (k+k_0)\Delta y, (l+l_0)\Delta \dot{y}, (m+m_0)\Delta\omega)^{\mathrm{T}}$, $i = 0,\ldots,N_x$, $j = 0,\ldots,N_{\dot{x}}$, $k = 0,\ldots,N_y$, $l = 0,\ldots,N_{\dot{y}}$, $m = 0,\ldots,N_\omega$ where $i_0,\ldots,m_0$ are offsets used to translate the origin. The total number of grid nodes is $(N_x+1)(N_{\dot{x}}+1)(N_y+1)(N_{\dot{y}}+1)(N_\omega+1)$ while the number of unknowns is $N = (N_x-1)(N_{\dot{x}}-1)(N_y-1)(N_{\dot{y}}-1)(N_\omega-1)$. Boundary conditions must be specified on this hyper-cube to determine the solution to the FPE uniquely. When the target has been localized the density should be concentrated in some small region and then decay exponentially far from this region. We assumed that the grid was large enough that the

density was small on its boundary. With this motivation we used a homogenous Dirichlet condition with the solution held at 0 on the boundary.

The FPE is a degenerate parabolic partial differential equation [Friedman] which means that it does not have second order derivatives in all of its variables. Specifically, there are no $x-$ and $y-$ diffusion terms in Eq. (14) and both A_1 and A_3 correspond to one-way wave equation operators. (For example A_1 generates a wave that propagates solutions along the x-axis with velocity $\dot{x}$.) For a first order operator of this sort the boundary condition is only specified on the incoming boundary as determined by the sign of $\dot{x}$. As a result, if boundary conditions are specified on all of the faces then the solution is over determined. We avoided this problem by only specifying a physical boundary condition on the incoming $x-$ and $y-$ faces.

Even though the physical boundary condition is only defined for incoming x and y, the discretization scheme Eq. (26 a,c) requires that the solution also be specified on the out-going faces as well. This requires so-called numerical boundary conditions. A simple boundary condition to implement is to extrapolate the solution at the out-going faces [Strikwerda]. For example, in the region with $\dot{x} > 0$, the face with $i = N_x$ is an out-going face. On this face we specified $q_{N_x}^{k+1} = q_{N_x-1}^{k+1}$. On the other hand, when $\dot{x} < 0$, the out-going face has $i = 0$ so $q_0^{k+1} = q_1^{k+1}$. These numerical boundary conditions can be incorporated into the Thomas tridiagonal solver without affecting its complexity.

2.4 Measurement Models

For this study we assumed that two distinct measurements types were available: HRR measurements $\mathbf{z}$ which depend on target bank angle θ and target heading φ; and position measurements $\mathbf{z}_p = (z_{xp}, z_{yp})$ which are Cartesian x, y with additive zero-mean white Gaussian errors of standard deviation σ_p. For simplicity both were assumed to be made at the same instant so that each measurement in Eq. (2) consists of the pair $\mathbf{y}_k = (\mathbf{z}, \mathbf{z}_p)_k$.

We used a scattering center model [Smith] for the HRR measurements. In this type of model the impulse-response function for target class T_c is approximated by

$$r_c(t) = \sum_s A_{cs}\delta(t - t_{cs}), \qquad (27)$$

where A_{cs} is the scattering amplitude of the s-th scattering center in targets of class T_c. The time delay t_{cs} is proportional to the range from the radar to the scattering center at the time of scattering. Let $\mathbf{x}_{cs}$ denote the 3-dimensonal Cartesian coordinates of a scattering center in the body frame of the target and $\mathbf{R}$ denote the vector from the radar to

the body frame origin. The rotation of the target from the body frame into the fixed frame of the radar was take to be

$$\Theta = \begin{pmatrix} \cos\varphi & \sin\varphi & 0 \\ -\cos\theta\sin\varphi & \cos\theta\sin\varphi & \sin\theta \\ \sin\theta\sin\varphi & -\sin\theta\cos\varphi & \cos\theta \end{pmatrix}. \tag{28}$$

This is the Euler rotation matrix in the so-called *x*-convention with the pitch angle $\psi = 0$. The 0-heading direction was taken to be along the *x*-axis. With this definition the time delay is

$$t_{cs} = \frac{2|\mathbf{R}|}{c} + \frac{2}{c|\mathbf{R}|}\mathbf{R}^{\mathrm{T}}\Theta\mathbf{x}_{cs}. \tag{29}$$

The first term is a total offset determined by the nominal range to the target. The second term is the projection of the scatterers onto the sensor-target unit vector. In HRR systems the target range must be estimated in order to properly align the HRR signatures. We assumed that the target signatures are already aligned. After digital sampling with range resolution ΔR the signature in range bin b is

$$r_c^b = \sum_s A_{cs}\mathrm{II}\left(b - \hat{\mathbf{R}}^{\mathrm{T}}\Theta\mathbf{x}_{cs} / \Delta R\right), \tag{30}$$

where

$$\mathrm{II}(x) = \begin{cases} 1, & |x| < 1/2 \\ 0, & \text{otherwise.} \end{cases} \tag{31}$$

Noise was added to the signatures to produce HRR measurements $z_b = r_c^b + n_c^b$ where $n_c^b \sim N(0, \sigma_{HRR})$. We assumed that the noise contributions to each bin are uncorrelated and white. A single HRR measurement is the vector $\mathbf{z} = (z_1, \ldots, z_B)^{\mathrm{T}}$. Therefore, the conditional density is

$$p(\mathbf{z}|\theta, \varphi, T_c) = \kappa\prod_b \exp\left(-(z_b - r_c^b)^2 / 2\sigma_{HRR}^2\right) \tag{32}$$

where κ is a constant that can be dropped.

Implementation of the classifier requires the density transformation

$$p(\mathbf{z}|\dot{x},\dot{y},\omega,T_c) = p(\mathbf{z}|\theta,\varphi,s,T)\left|\frac{\partial(\theta,\varphi,s)}{\partial(\dot{x},\dot{y},\omega)}\right|. \tag{33}$$

Using $s=\sqrt{\dot{x}^2+\dot{y}^2}$, $\theta=\text{atan}(\omega s/g)$, $\varphi=\text{atan}(\dot{y}/\dot{x})$,

$$\left|\frac{\partial(\theta,\varphi,s)}{\partial(\dot{x},\dot{y},\omega)}\right| = \frac{1}{g\left(1+\omega^2 s^2/g^2\right)} \tag{34}$$

so that

$$p(\mathbf{z}|\dot{x},\dot{y},\omega,T_c) = \frac{p(\mathbf{z}|\theta,\varphi,s,T_c)}{g\left(1+\omega^2 s^2/g^2\right)}. \tag{35}$$

Neglecting an irrelevant normalization factor, the measurement density required for the measurement update Eq. (8) is

$$\begin{aligned} p(\mathbf{y}|\mathbf{x},T_c) = &\frac{1}{\left(1+\omega^2 s^2/g^2\right)}\exp\left(-\left((z_{xp}-x)^2+(z_{yp}-y)^2\right)/2\sigma_p^2\right) \\ &\cdot\prod_b \exp\left(-(z_b-r_c^b)^2/2\sigma_{HRR}^2\right) \end{aligned} \tag{36}$$

where r_c^b as a function of $\mathbf{x}$ is given by Eq. (30).

2.5 Grid Translation

To reduce the size of the grid required to represent the target joint density, the grid was translated after each measurement to approximately maintain the target's location near its center. After each measurement update the target position estimate $(\hat{x}_t,\hat{y}_t)$ was evaluated using Eq. (5) and the grid was shifted to center of the grid near this position. This was achieved by placing the lower left corner of the spatial grid at (i_0,j_0) where

$$i_0 = \left[\hat{x}/\Delta x - N_x/2\right] \tag{37a}$$

$$j_0 = \left[\hat{y}/\Delta y - N_y/2\right] \tag{37b}$$

and $[x]$ denotes rounding to the nearest integer. This always translated the grid by an integral multiple of $(\Delta x,\Delta y)$. Grid nodes outside the intersection of the translated and un-translated grid were set to 0.

2.6 The Maximum Likelihood Classifier

As a basis for comparison we implemented a Maximum Likelihood Classifier (MLC) for target class without making use of pose information. This classifier only used the HRR measurements. It was computed recursively using

$$p(T_c|Z_{t_k}) = \frac{p(\mathbf{z}_{t_k}|T_c)\,p(T_c|Z_{t_{k-1}})}{\sum_{c'} p(\mathbf{z}_{t_k}|T_{c'})\,p(T_{c'}|Z_{t_{k-1}})}, \tag{38}$$

where measurement $\mathbf{z}_{t_k}$ is the HRR measurement only for time t_k and $Z_{t_{k-1}}$ denotes the HRR measurement set prior to time t_k (no kinematic measurements are used). The target state $\mathbf{x}_t$ was treated as a nuisance variable [Smith] and integrated out for each scan using

$$p(\mathbf{y}_k|T_c) = \int d\mathbf{x}_t\, p(\mathbf{y}_k|\mathbf{x}_t, T_c)\,. \tag{39}$$

3. Results

These algorithms for HRR signature modeling and classification were implemented in C++ . Scattering center models for two target types (F-16 and A-10 aircraft) were generated using between 15 and 20 scattering centers. The scattering amplitudes A_{cs} (c.f. Eq. (27)) were assumed real with locations taken from [Janes]. Heuristic scattering amplitudes were used and ranged in value from 0 to 4 units. Typical signature with range resolution $\Delta r = 1$ m are shown in Figure 2. The targets are at bank angle $\varphi = 0$ and rotated in heading θ about the forward part of the aircraft, which is held fixed at range bin 20. The sensor is assumed to be far to the west of the target so the sensor-target unit vector $\hat{R}$ in Eq. (30) is the east unit vector. The A-10 was modeled with the strongest scattering from the engines and empennage near range bin 10 at $\theta = 0$ and some scattering from the wings. The F-16 was modeled with the dominant scattering from the empennage and the engine inlet near the forward part of the aircraft which is located at range bin 16 at $\theta = 0$. The signatures were pre-computed and stored.

For testing purposes a third target signature was also used, referred to as the 'A-10.1'. The A-10.1 was obtained by perturbing the position and amplitude of the A-10 signature by adding Gaussian noise to it with a standard deviation of .1 m in each position component and .1 units in amplitude. HRR measurements were obtained from the signatures by adding zero-mean Gaussian noise with standard deviation σ_{HRR} to them. Measurements obtained from the signatures of Figure 2 with $\sigma_{HRR} = 2.5$ are shown in Figure 3.

The D'Yakonav scheme Eq. (25a-c) with homogeneous boundary conditions was used for a grid with $N_x = N_y = 8$, and $N_{\dot{x}} = N_{\dot{y}} = N_\omega = 12$. The grid resolution was $\Delta x = \Delta y = 100$ m , $\Delta \dot{x} = \Delta \dot{y} = 25$ m / s and $\Delta\omega = .0245$ rad / s . The plant noise values were $\sigma_{\dot{x}}{}^2 / 2 = \sigma_{\dot{y}}{}^2 / 2 = .001\ \mathrm{m}^2 / s^3$ and $\sigma_\omega{}^2 / 2 = .00001\ \mathrm{rad}^2 / s^3$. The total number of

unknowns was $N = 62{,}219$. On this grid the full filter required between 1 and 5 seconds per update on a single-processor engineering workstation.

Figure 4 shows the average classification probability versus time for this 3-class test problem (A-10, A-10.1, F-16) obtained over 100 trials each for $\sigma_{HRR} = 2,\ 2.5,\ 3$ using the NLFJTR classifier (upper curves) and the MLC. The true target class was the A-10 with speed 100 m/s and turn rate $\omega = .098$ rad / s (1g acceleration). The sensor update rate was 1 Hz. The Cartesian position measurements were obtained by adding zero-mean Gaussian noise to the target position with standard deviation $\sigma_p = 100 / \sqrt{12}$ m ≈ 28.9 m. The NLF was initialized with the target position and velocity localized to a single resolution cell. No prior turn rate information was assumed and its initial density was taken as uniform. In all cases NLFJTR yielded a high correct classification probability sooner than the MLC. The target state estimates obtained from Eq. (5) for the $\sigma_{HRR} = 2.5$ case are shown in Figure 5. This shows the time dependence of the true and estimated position, velocity and turn rate, averaged over 100 trials. Over this trial set the RMS position error was 31 m, the RMS velocity error was 19.5 m/sec, and the RMS turn rate error was .032 rad/s.

4. Discussion

The classification probability results using Nonlinear Filtering for Joint Tracking and Recognition (NLFJTR) and the Maximum Likelihood Classifier (MLC) shown in Figure 4 demonstrate that performance can be improved by using kinematic and signature measurements in single recursive filter. Identical data models were used for both classifiers so the difference between them can be attributed to NLFJTR's fusion of position measurements with High Range Resolution Radar (HRR) measurements allowing it to estimate target pose while the MLC assumed pose to be independent from scan to scan and only derived pose information from the HRR data itself.

The main objective of this work has been to demonstrate the feasibility and utility of using NLF methods for recursive joint tracking and recognition. The D'Yakonov ADI scheme used here to solve the Fokker-Plank Equation (FPE) Eq. (14) is one of many related schemes that can be used for NLF applications. One possible draw-back is that while the D'Yakonov scheme is $O(\Delta t^2)$ accurate in time, it is non-dissipative [Strikwerda]. This means that there is no damping of high-frequency errors in the FPE solution and small errors can persist over time. An alternative approach that address this issue would be to take the implicit Euler scheme as the starting point for solving the FPE. Even though the implicit Euler scheme is $O(\Delta t)$ accurate and more time steps may be required for solution to a given level of accuracy, its dissipative damping of high-frequency error components may outweigh this disadvantage. On the other hand, NLF applications differ from conventional partial differential equation problems in that the solution is periodically modified by the Bayes' rule update Eq. (8) which has a stabilizing effect. Dissipative schemes with $O(\Delta t^2)$ accuracy can also be constructed, although

they are more complicated which may cause implementation difficulties on domains of dimension 4, 5, and higher as required for NLFJTR.

A similar issue related to the dissipativity of the solution scheme is the discretization scheme used for the first order spatial derivatives. We chose to use central differencing for $A_{i\Delta\mathbf{x}}$ Eq. (26a,c) which is $O(\Delta\mathbf{x}^2)$ accurate. However, for non-smooth initial data, so-called up-wind differencing schemes can perform better [Press, Strikweda]. Unfortunately, in its simplest form the up-wind scheme is only $O(\Delta\mathbf{x})$ accurate. Again, while $O(\Delta\mathbf{x}^2)$ accurate up-wind schemes exist, they complicate filter implementation.

Another topic for further study is the boundary conditions used for the FPE. The turn-rate estimate in Figure 5c was consistently biased low. This may be due to the loss of probability through the ω-faces of the grid. We used the homogeneous Dirichlet conditions on all boundaries, which assumes that the discrete finite domain used for the numerical solution is large enough that the true FPE solution is nearly zero on its boundary. One alternative would have been to use Neumann conditions requiring 0 probability flux across the boundaries. However, in either case there is some perturbation of the density near the boundary analogous to the probability distortion caused by gating in conventional trackers. It may be better to use some lower order scheme to approximate the solution on the boundary. A simple way to do this would be to approximate the density on the boundary using an extended Kalman filter, then use the numerical FPE solver with the resulting inhomogenous boundary condition. This is a Gaussian boundary approximation but does not lead to a Gaussian interior solution when the initial condition is non-Gaussian. A more sophisticated method would be to use multiple resolution grids. With this approach the grid for the region of interest is embedded in a larger, coarser grid [Schaffer]. The solution on the coarse grid is obtained using the numerical solver and then the boundary condition for the fine grid is obtained from the coarse grid solution. The fine grid problem is then solved with the resulting inhomogenous boundary condition.

The grid translation scheme used here was simple to implement but greatly reduced the computation required for this problem since it allowed a much smaller grid to be used. We only translated the grid in the spatial components, but translation in velocity can also be performed with a slight modification to the FPE solver. It may also be useful to scale the grid, based, say, on estimated standard deviation of the solution as obtained from the 2nd moment evaluations. This would allow a much smaller grid to be used although it may require more careful treatment of the boundary conditions along the lines noted above.

Data modeling is a critical issue for applying NLFJTR algorithms to more realistic problems. Physics-based signature modeling is currently a very high investment area, although there are those within the ATR community that regard physical modeling of HRR signature models as fundamentally unfeasible. The data model used in this algorithm study is quite crude but this approach can incorporate higher fidelity models without modification. This can include signature probability densities obtained from high

fidelity models, estimated from actual target observations or from scaled model data taken in anechoic chambers. For this test problem we calculated the signature density directly as a function of the range profile but computation may be simplified by using some form of dimensionality reduction by projecting the range profiles onto an optimized space of lower dimensionally. For example, [Zyweck] use linear discriminants obtained using statistical cluster analysis techniques while [Mitchell-2] use nonlinear statistical features. We employed a deterministic signature model in this work but can incorporate the conditionally Gaussian models suggested in the work of [Jacobs]. Also, even though we chose to model the signature noise as Gaussian, this is not a requirement of the algorithm. Based on physical arguments the true distribution should be Rician [Mitchell-1], or at least have a Rician component which is easily accommodated within this algorithm. The critical requirement for using these signature modeling alternatives in NLFJTR is that a probability to observe a signature given target class and kinematic state analogous to Eq. (32) can be represented to some level of accuracy.

Acknowledgment: The authors benefited from discussions with A. Friedman, N. Krilov, E. Libby, S. Musick, J. O'Sullivan, C. Poling, B. Rozovsky, and S. Schaffer regarding this work.

References:

1. [Andrisani] D. Andrisani, E. T. Kim, J. Shierman, F. P. Kuhl, (1991), "A Nonlinear Helicopter Tracker Using Attitude Measurements", *IEEE Trans. Aerosp. Electron. Syst.*, Vol. 27, No. 1, January 1991, pp. 40-47.

2. [Berman] A. Berman, E. C. Chen, W. B. Kessler, R. K. Klinger, C. Lau., J. K. Liu, H. N. Nussbaum, W. Sandius, H. D. Washburn, (1993), "Production and Classification of Advanced Radar Signatures Using the APG-71 Fire Control Radar Produced for the F-14 Aircraft" (U), *Proceedings of 39th Tri-Service Radar Symposium*, 1993, pp. 183-194, (SECRET/NOFORN).

3. [Daum] F. E. Daum, "Solution of the Zakai Equaiton by Separation of Variables", *IEEE Trans. Aerosp. Electron. Syst.*, Vol. AC-32, No 10, Oct. 1987, pp. 941-943.

4. [Friedman] A. Friedman, "Uniqueness for the Cauchy Problem for Degenerate Parabolic Equations", *Pacific Journal of Mathematics*, Vol. 46, No. 1, 1973.

5. [Fukunaga] K. Fukunaga, *Introduction to Statistical Pattern Recognition*, Academic Press Inc., Boston, 1990.

6. [Greengard] L. Greengard, "Fast Algorithms for Classical Physics", *Science*, Vol. 265, 12 Aug. '94, pp. 909-914.

7. [Ho] Y. C. Ho, R. C. K. Lee, "A Bayesian Approach to Problems in Stochastic Estimation and Control", *IEEE Trans. Auto. Cont.*, Vol. 19, Oct., 1964, pp. 333-339.

8. [Iny] D. Iny, M Morici, M. Souders, (1994), "Quantitative Methods in HRR NCTR and Their Application to Training Data Issues", CISC-94.

9. [Janes] *Jane's All the World's Aircraft 1996-1997*, Jane's Information Group, Surrey, UK, 1996.

10. [Jacobs] S. Jacobs, J. A. O'Sullivan, "High Resolution Radar Models for Joint Tracking and Recognition", *Proceedings of the 1997 IEEE National Radar Conference*, May, 1997, pp. 99-104

11. [Jazwinski] A. H. Jazwinski, 1970, *Stochastic Processes and Filtering Theory*, Academic Press, New York.

12. [Kendrick] J. D. Kendrick, P. S. Maybeck, J. G. Reid, "Estimation of Aircraft Target Motion Using Orientation Measurements", *IEEE Trans. Aerosp. Electron. Syst*., Vol. AES-17, No. 2, March 1981, pp. 40-47.

13. [Kastella] K Kastella, M. A. Kouritzin and A. Zatezalo, "A nonlinear filter for altitude tracking", October 1996 *Proceedings of the Air Traffic Control Association* pp. 1-5

14. [Kouritzin] M. A. Kouritzin, "On exact filters for continuous signals with discrete observations", Technical Report #1409, University of Minnesota Institute for Mathematics and Its Applications, May 1996; to appear in *IEEE Trans. on Aut. Control*

15. [Larson] R. E. Larson, J. Peschon, "A Dynamic Programming Approach to Trajectory Estimation", *IEEE Trans. Auto. Cont.*, Vol. 11, No. 3, July 1966, pp. 537-540.

16. [Le Chevalier] F. Le Chevalier, *et al*, "Radar Target and Aspect Angle Identification", *Proceedings of the IEEE 1978 International Conference on Pattern Recognition.* pp. 398-400, 1978.

17. [Libby] E. W. Libby, P. S. Maybeck, "Sequence Comparison Techniques Multisensor Data Fusion and Target Recognition", IEEE Trans. Aero. El. Sys., Vol 32, No 1, Jan. 1996, pp. 52-65.

18. [McCormick] S. F. McCormick (ed.), *Multigrid Methods: Theory, Applications and Supercomputing*, Marcel Dekker, New York 1988.

19. [Mieras] H. Mieras, T. Cichocki, "Airframe Identification Results Using High Range Resolution", *1990 Joint Service Combat Identification Conference Technical Proceedings* (U), D. Youngberg (ed.), pp. 1107-1115, 1990 (SECRET/NOFORN).

20. [Miller] M. I. Miller, A Srivastava, U. Grenander, "Conditional-Mean Estimation Via Jump-Diffusion Processes in Multiple Target Tracking/Recognition", *IEEE Trans. Aerosp. Electron. Syst.*, Vol. 43, No. 11, Nov. 1995, pp. 2678-2690.

21. [Mitchell-1] R. A. Mitchell, R. DeWall, "Overview of High Range Resolution Radar Target Identification", Wright Laboratories internal report.

22. [Mitchell-2] R. A. Mitchell and J. J. Westerkamp, "A Statistical Feature Based Classifier for Robust High Range Resolution Radar Target Identification", submitted to *IEEE Trans Aero. Elect. Sys.*, Nov. 97.

23. [O'Sullivan] J. A. O'Sullivan, K. C. Du, R. S. Teichman, M. I. Miller, D. L. Snyder, V. C. Vannicola, "Radar Target Recognition Using Shape Models", *Proceedings of the Thirtieth Allerton Conference on Communication, Control and Computing*, Urbanna, IL, October, 1992.

24. [Press] W. H. Press, S. A Teukolsky, W. T. Vetterling, B. P. Flannery, *Numerical Recipes in C - Second Edition*, (1992), Cambridge University Press.

25. [Rozovskii] Lototsky, C. Rao, and B.L. Rozovskii, ’’Fast nonlinear filter for continuous-discretetime multiple models’’,Proc. 35th IEEE Conf. on Decision and Control, Kobe, Japan, 1996, pp.4060-4064; S. Lototsky, R. Mikuleviclus, B. L Rozovskii, "Nonlinear Filtering Revisited: A Spectral Approach", *SIAM J. Contr. Optim*., Vol. 35, No.2, March 1997; S.Lototsky, B. L. Rozovskii, "Recursive Nonlinear Filter for a Continuous-Discrete Time Model: Separation of Parameters and Observations" IEEE Trans Aut. Con 1998 (to appear).

26. [Schaffer] S. Schaffer, personal communication.

27. [Sorenson] H.W. Sorenson, “On the Development of Practical Nonlinear Filters,” *Information Sciences*, Vol. 7, 1974, pp. 253-270. -----, “Recursive Estimation for Nonlinear Dynamic Systems,” in J.C. Spall, ed., *Bayesian Analysis of Time Series and Dynamic Models*, Marcel Dekker, 1988, pp. 127-165.

28. [Smith] C. R. Smith and P. M. Goggans, "Radar Target Identification", IEEE Antennas and Propagation Magazine, Vol. 35., No. 2, April 1993, pp. 27-37.

29. [Strikwerda] J. C. Strikwerda, *Finite Difference Schemes and Partial Differential Equations*, Chapman & Hall, New York, 1989.

30. [Wehner] D. R. Wehner, *High Resolution Radar*, Artech House, Inc., Norwood, MA, 1987.

31. [Yanenko] N. N. Yanenko, *The Method of Fractional Steps*, Springer-Verlag, 1971.

32. [Zatezalo] A. Zatezalo, *Tracking and Detection for the Target State Model*, University of Minnesota M. S. Thesis, March 15, 1997.

33. [Zyweck] A. Zyweck and R. E. Bogner, "Radar Target Classification of Commercial Aircraft", *IEEE Trans Aero. Elect. Sys.*, Vol. 32, No. 2, April 1996, pp. 598-606.

Information flow in uncoupled NCTI algorithms for HRRR

a)

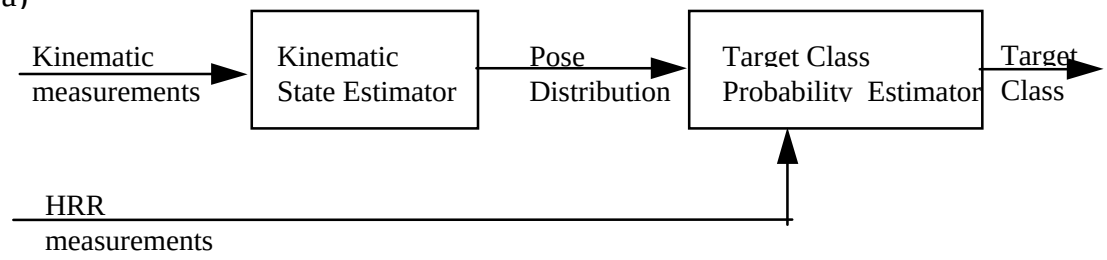

Information flow in coupled NCTI algorithms

b)

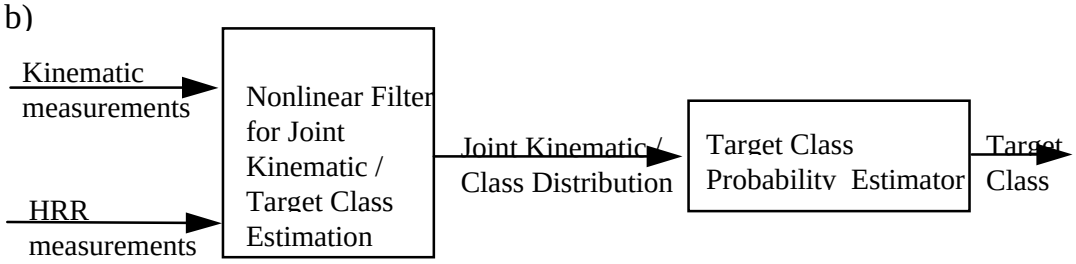

Figure 1 -- Information Flows in NCTI Uncoupled algorithms (a) first extract target orientation information from kinematic measurements and then combine it with HRR measurements to determine target class. Coupled algorithms (b) combine HRR measurements with kinematic data in a single filter to compute the joint kinematic / class density allowing 2-way feedback between kinematics and HRR signatures. Target class probability is obtained as a marginal distribution from the joint density.

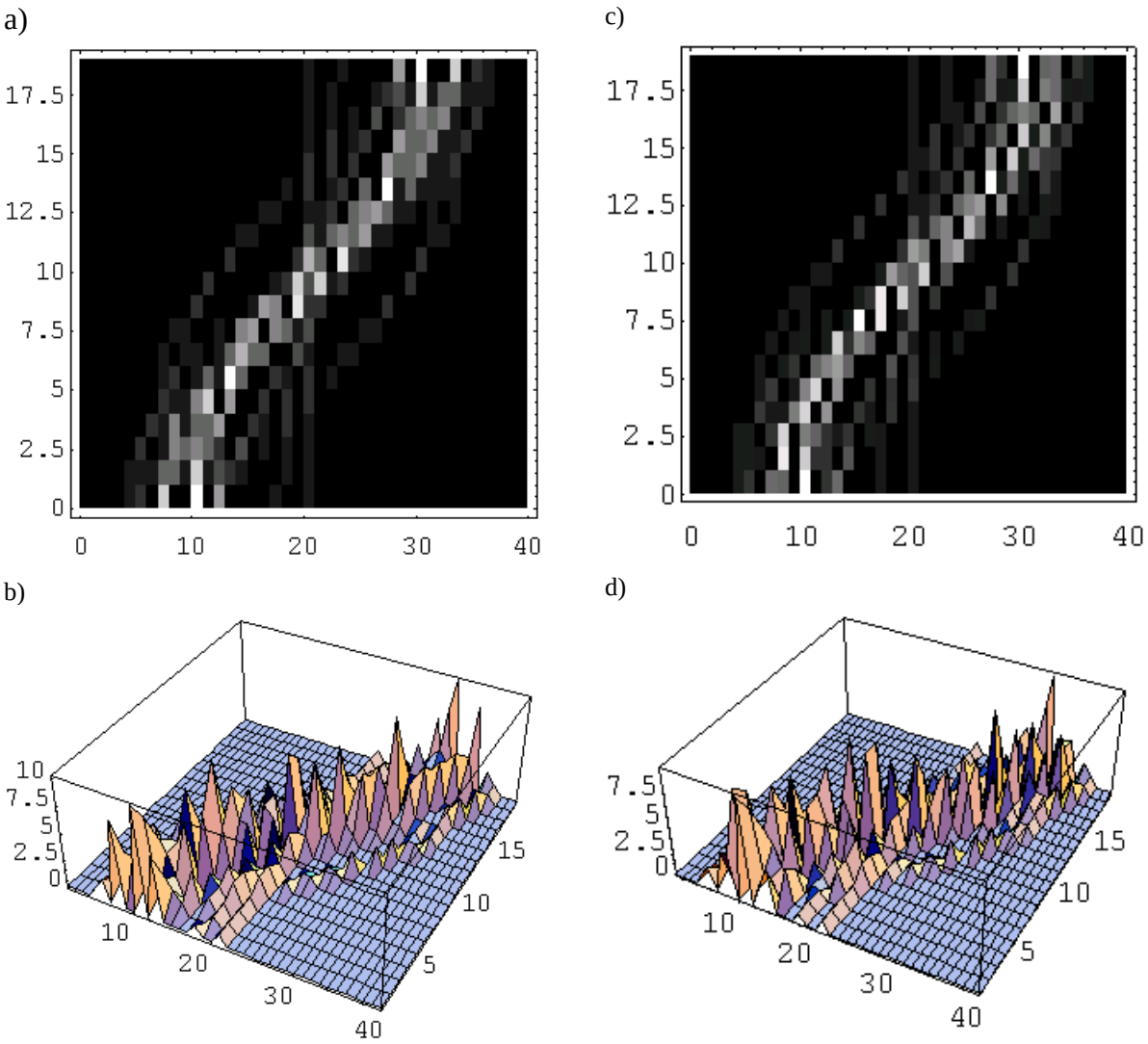

Figure 2 - Simulated HRR signatures for the A-10 (a, b) and the F-16 (c, d). The targets are at 0 bank angle, range bin is plotted across the page and heading angle varies form 0 to 180^0.

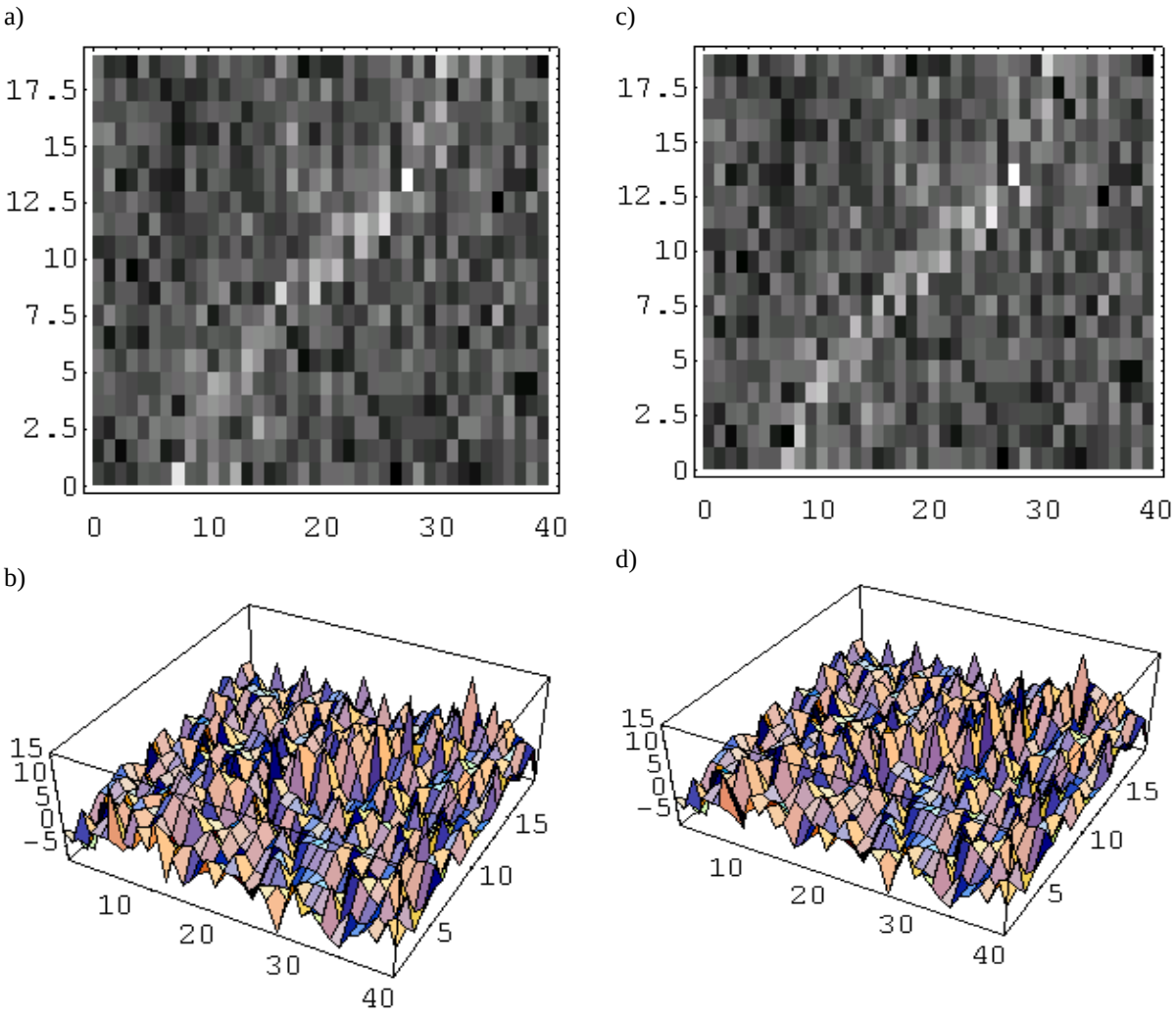

Figure 3 - Simulated HRR measurements obtained from the signatures of Figure 2 by adding Gaussian noise with variance $\sigma_{HRR} = 2.5$.

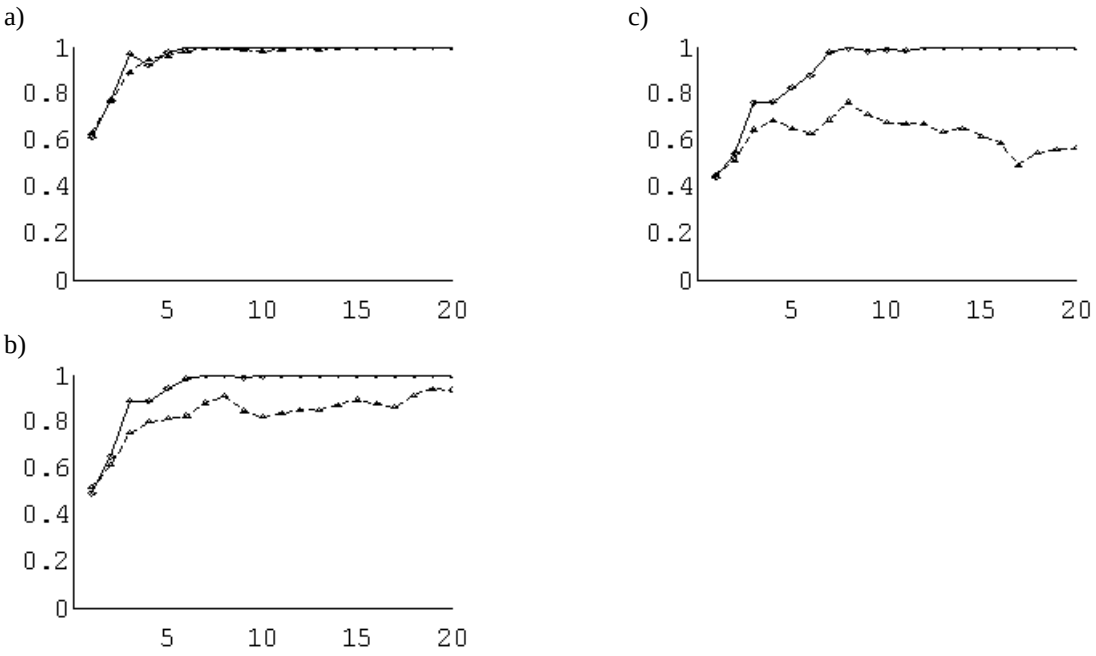

Figure 4 – Average classification probability P_c versus sample time plotted across the page using Joint Tracking and Recognition (upper curves) and using a Maximum Likelihood Classifier with measurement noise $\sigma_{HRR} = 2$ (a) $\sigma_{HRR} = 2.5$ (b), and $\sigma_{HRR} = 3$ (c), averaged over 100 Monte Carlo trials.

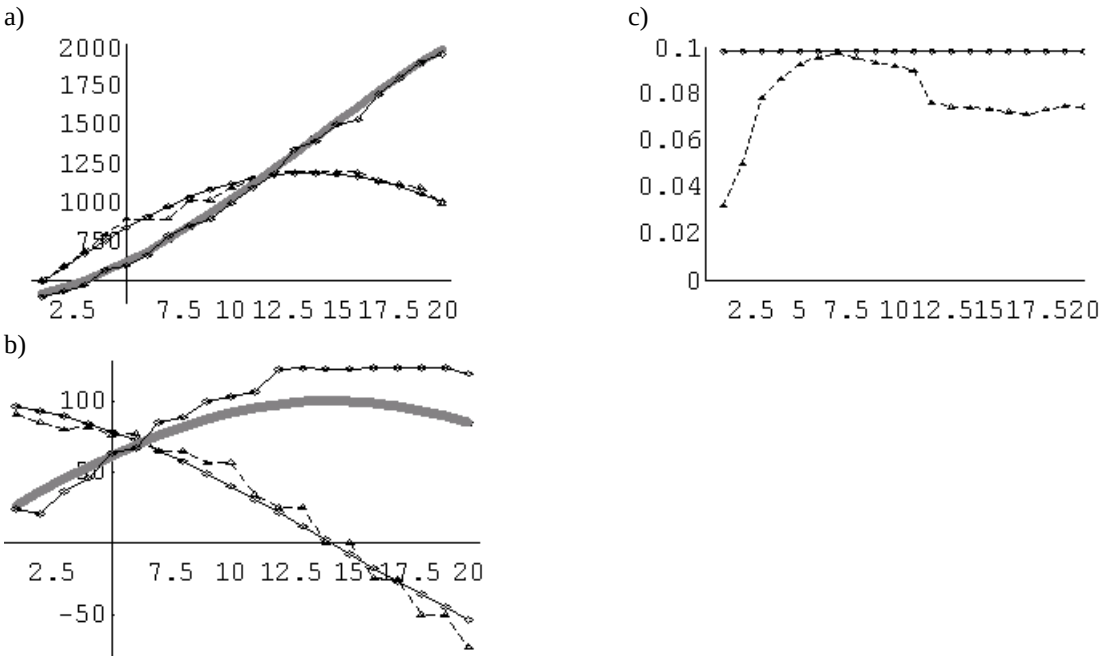

Figure 5 – True target state (smooth curves) and state estimates obtained using Joint Tracking and Recognition with signature measurement noise $\sigma_{HRR} = 2.5$ for position (a), velocity (b) and turn rate (c).